EUROPEAN SYNCHROTRON RADIATION FACILITY

INSTALLATION EUROPEENNE DE RAYONNEMENT SYNCHROTRON

ESRF

Experiment Report Form

The double page inside this form is to be filled in by all users or groups of users who have had access to beam time for measurements at the ESRF.

Once completed, the report should be submitted electronically to the User Office via the User Portal:

https://wwws.esrf.fr/misapps/SMISWebClient/protected/welcome.do

Reports supporting requests for additional beam time

Reports can be submitted independently of new proposals – it is necessary simply to indicate the number of the report(s) supporting a new proposal on the proposal form.

The Review Committees reserve the right to reject new proposals from groups who have not reported on the use of beam time allocated previously.

Reports on experiments relating to long term projects

Proposers awarded beam time for a long term project are required to submit an interim report at the end of each year, irrespective of the number of shifts of beam time they have used.

Published papers

All users must give proper credit to ESRF staff members and proper mention to ESRF facilities which were essential for the results described in any ensuing publication. Further, they are obliged to send to the Joint ESRF/ ILL library the complete reference and the abstract of all papers appearing in print, and resulting from the use of the ESRF.

Should you wish to make more general comments on the experiment, please note them on the User Evaluation Form, and send both the Report and the Evaluation Form to the User Office.

Deadlines for submission of Experimental Reports

- 1st March for experiments carried out up until June of the previous year;
- 1st September for experiments carried out up until January of the same year.

Instructions for preparing your Report

- fill in a separate form for each project or series of measurements.
- type your report, in English.
- include the reference number of the proposal to which the report refers.
- make sure that the text, tables and figures fit into the space available.
- if your work is published or is in press, you may prefer to paste in the abstract, and add full reference details. If the abstract is in a language other than English, please include an English translation.

ESRF	**Experiment title:** Evaluation of the SRO/MRO of metastable alloys with nanoscale heterogeneities	**Experiment number**: HD 482
Beamline: ID 11	**Date of experiment**: from: 27.01.2011 to: 1.02.2011	**Date of report**: 1.03.2011
Shifts: 15	**Local contact(s)**: Dr VAUGHAN Gavin	*Received at ESRF:*

Names and affiliations of applicants (* indicates experimentalists):

Dr. STOICA Mihai*
Prof. ECKERT Jürgen
Director YAVARI A.R.*

Report:

Bulk metallic glasses (BMGs) usually undergo thermal embrittlement, or more precisely, an increase to above room temperature of the temperature of onset of ductility (ductile–brittle transition temperature T_{db})) due to loss of the quenched-in excess free volume $V_{excess\text{-}f}$ [1]. Furthermore, most metallic glasses become brittle upon crystallization after annealing to temperatures higher than their crystallization temperatures (T_x) [2]. However, some Fe-B based metallic glasses remain ductile even after crystallization [3, 4]. For example $Fe_{83}B_{17}$ metallic glass remains ductile after annealing in the temperature range of 458-505^{o}C, above its crystallization temperature (T_x = 458^{o}C), while annealing above 505^{o}C results in the embrittlement of this alloy. In order to understand this exceptional behavior, the crystallization process of $Fe_{83}B_{17}$ was studied in situ, by heating this metallic glass in the synchrotron beam while acquiring x-ray diffraction patterns, Fig 1. By combining these results with TEM observations (Fig 2 a and b) of annealed samples at different temperatures and DSC measurements, we concluded that the first crystallization event of $Fe_{83}B_{17}$ at 458^{o}C results in a composite structure containing amorphous phase and nanocrystals of α-Fe and the metastable $Fe_{23}B_6$ intermetallic phase. The embrittlement of the annealed metallic glass observed at annealing temperatures higher than 505^{o}C is related to grain growth of the precipitated nanocrystals as well as to the decrease of the volume fraction of the amorphous matrix. Annealing at temperatures above 535^{o}C leads to full crystallization of this metallic glass and the main crystallization products are the metastable $Fe_{23}B_6$ phase, the intermetallic Fe_3B and α-Fe.

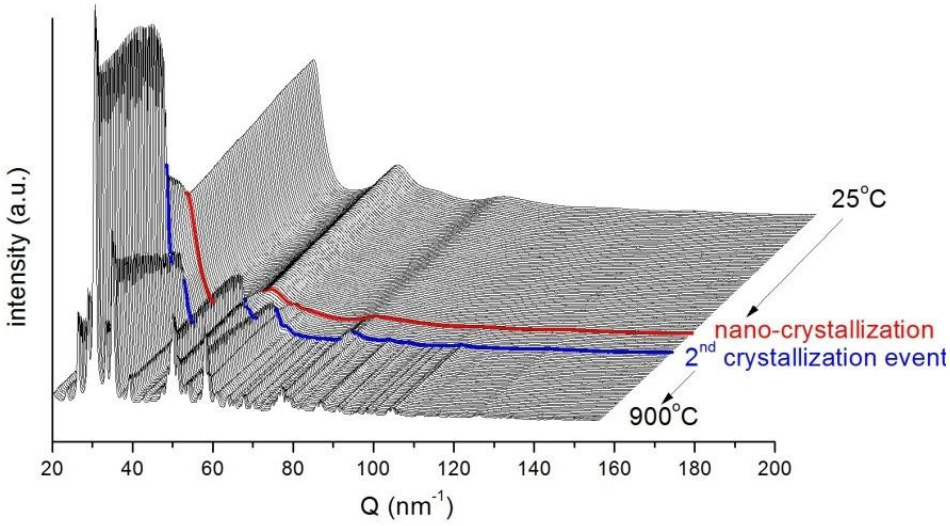

Fig. 1a: XRD spectra obtained during in situ annealing of the $Fe_{83}B_{17}$ metallic glass

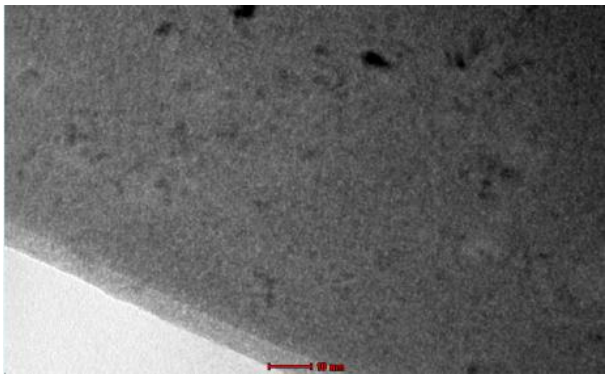

Fig. 2(a): $Fe_{83}B_{17}$ annealed at 474°C/ ductile

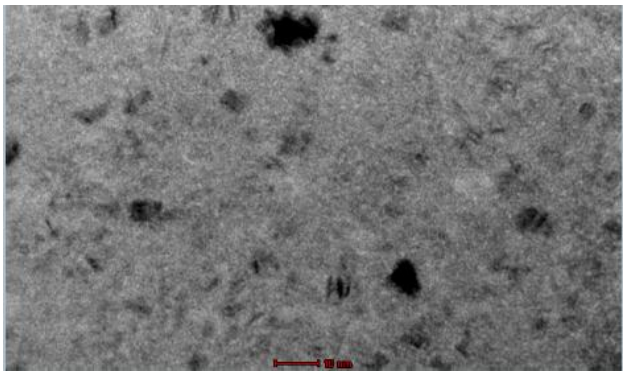

Fig. 2(b): $Fe_{83}B_{17}$ annealed at 505°C/ brittle

It is believed that the amorphous $Fe_{83}B_{17}$ phase does not undergo thermal embrittlement in the glassy state due to the high fraction of structural free volume, which unlike the quenched-in free volume, cannot be annihilated by thermal treatment. This structural free volume is related to the low atomic packing density resulting from the filling of the interstitial space between the host skeleton Fe atoms with B atoms. However, it has been shown [3] that FeB binary metallic glasses with higher B contents are brittle even in the as quenched state, implying higher atomic packing densities and low fraction of structural free volume when the metalloid contents begin to saturate the available interstitial sites in the disordered iron skeleton. Using real space pair distribution functions (PDFs) derived from high precision X-ray diffraction data collected at ID11, we attempt to probe the internal structure of FeB metallic glasses and analyze the structural differences of hypo- and hyper- eutectic FeB metallic glasses in the compositional range $Fe_{1-x}B_x$ ($15 < x < 25$).

As mentioned previously, the use synchrotron X-ray diffraction (XRD) enables to characterize the behaviour of atomic structure at elevated temperature in terms of scattered intensity and atomic pair correlation functions [5]. The variation of the position of the first diffuse diffraction peak in reciprocal space was proposed to be used in order to analyse the thermal expansion and to determine the fraction of free volume in metallic glasses [6]. The method was applied afterwards by several authors for different glassy metallic alloys [7-16]. With the help of x-ray diffraction in transmission configuration at ID11 we analysed the temperature dependence of the diffraction patterns of differently mechanically treated $Pd_{40}Cu_{30}Ni_{10}P_{20}$ glassy powders and to correlate reciprocal space data with thermal expansion, glass transition and structural relaxation. The investigations had to clarify certain discrepancies between the different reports with respect to the behaviour of the structure factor below and above the glass transition [5, 6] as well as for the influence of structural relaxation on the structure factor [17, 18]. Special care was done to avoid systematic errors in determination of diffraction maxima positions. Samples of $Pd_{40}Cu_{30}Ni_{10}P_{20}$ bulk glasses were prepared in form of rods with 5 mm diameter and 50 mm length by copper mould casting of the pre-alloy from the pure elements and refined by fluxing in B_2O_3. In order to study the structural relaxation, different rod shaped samples were milled under inert atmosphere for different times in a planetary micro mill Fritsch Puverisette and/or Retsch

planetary ball mill, at our home institute (IFW Dresden). The glassy $Pd_{40}Cu_{30}Ni_{10}P_{20}$ powders of about 100 µm particle size were mixed with NIST Al_2O_3 as internal standard and filled into glass capillaries.
Figure 3 shows the synchrotron XRD patterns $I(q)$ of the 5 samples at room temperature. Beside the diffuse maxima of the glassy $Pd_{40}Cu_{30}Ni_{10}P_{20}$ BMG, a diffuse maximum at $q_0 \approx 14.7$ nm^{-1} can be seen originating from scattering of the glass window of the hot stage as well as several weak reflections from the added Al_2O_3 powder. The applied temperature procedure for samples 1-3 and 5 is given by the inset of Fig. 3. First, the temperature was increased up to 622 K which is 53 K above the caloric glass transition temperature, then decreased to 360 K and finally heated up to 673 K which is above the crystallization temperature (sample 4: 53K - 573K - 360K - 673K). Figure 4 shows for two samples the behaviour of the positions of the first and second diffuse maximum at q_1 and q_2, the (116)-reflection of Al_2O_3 internal standard q_3 and of the window scattering of the hot stage at q_0. The positions of the maxima were calculated by a fit of Pseudo-Voigt functions. Because the window of the hot stage does not change its temperature, q_0 stays constant and gives evidence of the stability of the X-ray beam. The statistic analysis of the scatter in peak position q_0 of 300 measurements gives a standard deviation ± 0.01 nm^{-1}. For the somewhat sharper first diffuse peak of $Pd_{40}Cu_{30}Ni_{10}P_{20}$ glass a standard deviation of ± 0.005 nm^{-1} is estimated for q_1 ($2\theta_{max} = 3.302° \pm 0.001°$). The positions of the diffraction peaks corresponding to the sample follow the thermal cycling procedure (Fig. 4). During heating the maxima positions q_1 and q_3 shift to smaller q-values and, upon cooling to higher respectively. The position of the second maximum at q_2 exhibits a different behaviour altering the direction of the temperature dependence at T_g. First q_2 shifts to lower q-values with temperature. However, above T_g we observed for q_2 a reversed temperature dependence (Fig.4). Small differences of the maximum position between the two $Pd_{40}Cu_{30}Ni_{10}P_{20}$ samples are also reflected by the internal standard Al_2O_3 reflection. For crystalline materials the linear thermal expansion coefficient α of a inter-atomic spacing r_i can be calculated from the slope $\partial q_i(T)/\partial T = -\partial r_i(T)/\partial T = -\alpha * q_i$ because $q_i = 2\pi/r_i$. For the (116)-lattice plane of the Al_2O_3 standard a value of $\alpha = 7.2*10^{-6}$/K is obtained which is in a good agreement with $\alpha = 7.1 \cdot 10^{-6}$/K calculated from the temperature dependence of the lattice parameters of Al_2O_3 single between 300 and 600 K reported in [19].

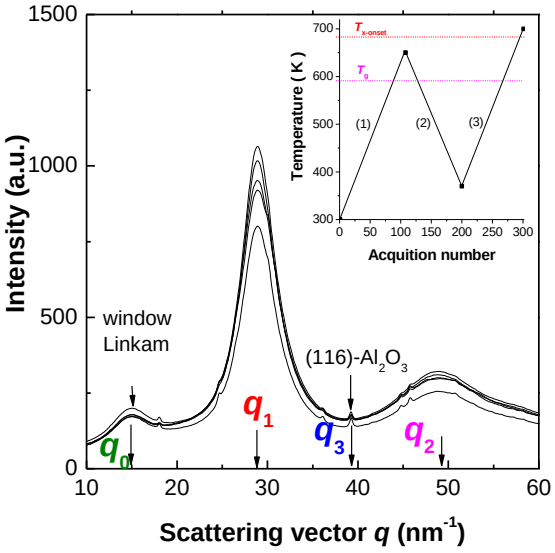

Fig.3: XRD patterns of $Pd_{40}Cu_{30}Ni_{10}P_{20}$ BMG powders and temperature cycles (inset)

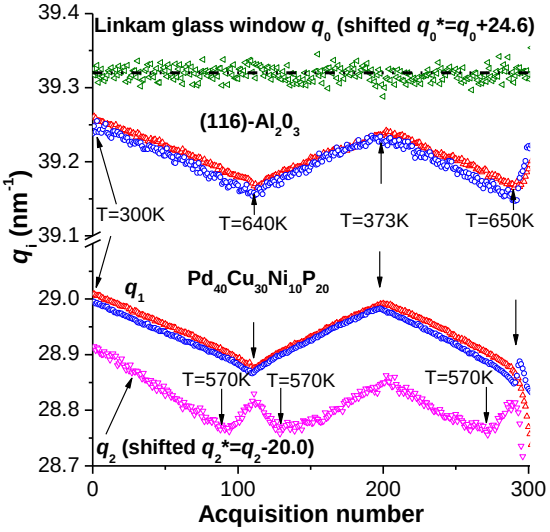

Fig.4: Maximum positions of $I(q)$ of two $Pd_{40}Cu_{30}Ni_{10}P_{20}$ BMGs upon temperature cycling

Besides the mentioned samples, several other Fe-based BMGs were investigated, in order to rule out the possible structural transformation during heating or to elucidate the free-volume theory. Following the experimental conditions as described previously (i.e. in-situ diffraction data acquisition during heating, cooling and subsequent heating), Fig. 5 shows the results about the volume variation for an $Fe_{74}Mo_4P_{10}C_{7.5}B_{2.5}Si_2$ BMG.

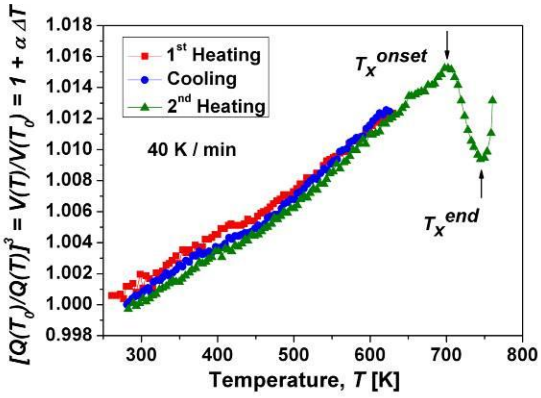

Fig. 5 (a) Volume variation in the case of 40-40-40 K/min heating-cooling-heating procedure.

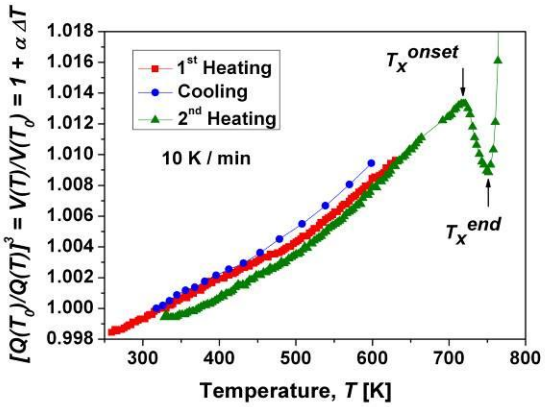

Fig. 5 (a) Volume variation in the case of 10-100-10 K/min heating-cooling-heating procedure.

In order to eliminate the possible errors of the proposed method, the heating-cooling-heating procedures were done at different heating and cooling rates. Fig. 5 (a) shows the case of heating-cooling-heating with 40-40-40 K/min, while the rates used for the data presented in Fig. 5 (b) were 10-100-10 K/min. There it is interesting to see that, in both cases, no free volume annihilation was observed. The curves reversible changes at 515 K the slope. It is interesting to point out that the respective temperature corresponds to the Curie temperature, i.e. order-disorder transition. It should be mentioned here that the measured samples were as-cast bulk samples. When powder amorphous samples obtained upon mechanical alloying (MA) were measured, the things are different and there a relatively large relaxation prior crystallization could have been observed (see Fig. 6). There a variation in volume of almost 1 % was observed.

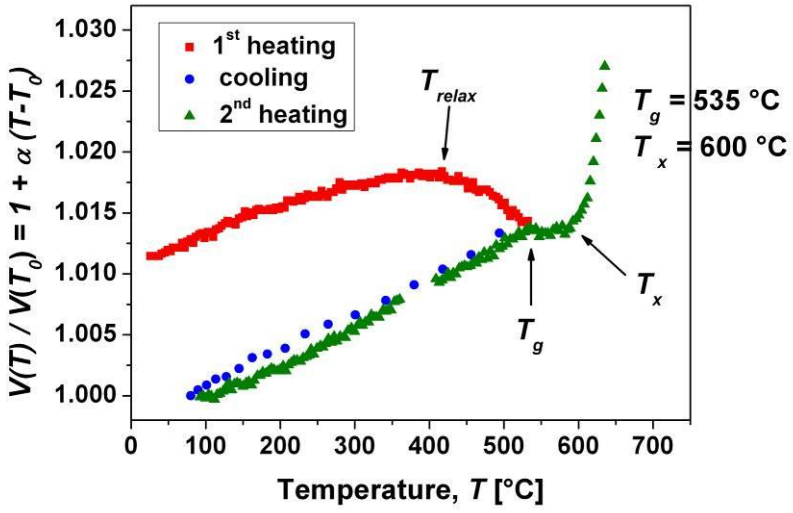

Fig. 6: Volume change as a function of temperature for a MA Co-based glass

With the help of the Linkam hot-stage several samples were annealed (nanocrystallized) in the beam. It is known that brittle BMGs may become deformable if there composite structures are formed. The method is efficiently only if the crystalline phase embedded in the residual amorphous matrix is in the nanometre range. For that, cylindrical samples already prepared at the home institute (IFW Dresden) were heated until the nanocrystallization event was observed. Fig. 7 (a) shows the behaviour of three similar samples of $\{[(Fe_{0.5}Co_{0.5})_{0.75}B_{0.20}Si_{0.05}]_{0.96}Nb_{0.04}\}_{100-x}Cu_x$ glass matrix composites. There was interesting to observe that only for x = 0.5 the procedure works. This is strictly related to the chemical composition of the starting BMGs. However, the procedure works, as it is shown also in Fig. 7 (b). There are two different samples of the same composition, showing a similar behaviour.

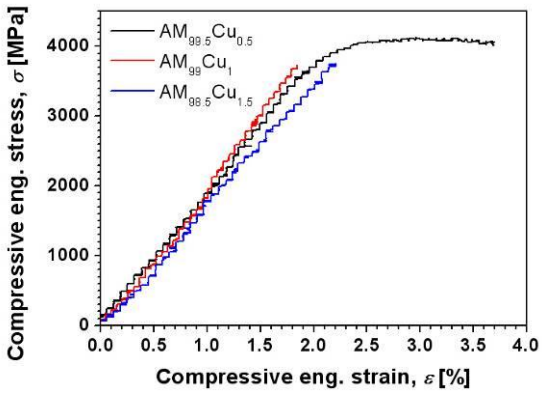

Fig. 7 (a): The ductile behaviour of $\{[(Fe_{0.5}Co_{0.5})_{0.75}B_{0.20}Si_{0.05}]_{0.96}Nb_{0.04}\}_{100-x}Cu_x$ glass matrix composites. AM stands for "Alloy Master", i.e. the parent composition $[(Fe_{0.5}Co_{0.5})_{0.75}B_{0.20}Si_{0.05}]_{96}Nb_4$.

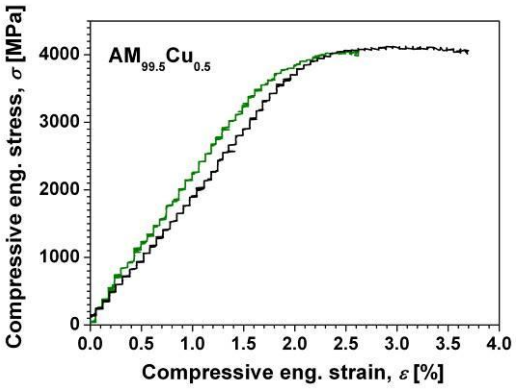

Fig. 7 (b): Two samples annealed in the beam at ID11 showing similar behaviour.

In order to illustrate in details the correlation between structural inhomogeneity originated from quenching and the ductility for BMGs, a simpler system was chosen. It is known that the radial distribution function is almost impossible to be calculated for BMGs which contains elements with strong interaction between them- and especially when there are more than 4 different elements. For this objective, $Cu_{47.5}Zr_{47.5}Al_5$ BMG was chosen. By carefully adjusting the melting current during quenching, $Cu_{47.5}Zr_{47.5}Al_5$ BMG with different internal state can be fabricated. On the other hand, binary $Cu_{100-x}Zr_x$ (x = 34, 35 and 36) were chosen to check the underlying correlation between structure change induced by rolling and ductility of BMGs. Furthermore, the binary system is easy to be analyzed due to its relatively simple microstructure [20]. The structural characteristic of CuZr-based BMGs are investigated by time-resolved in situ XRD performed at the ID 11 beam line at the European Synchrotron Radiation Facilities (ESRF, Grenoble, France) using a high-intensity, high energy monochromatic beam with a wavelength of 0.017615 nm. Compressive tests at room temperature were performed on a universal tension/compression testing machine (Instron 5869) equipped with a laser extensometer (Fiedler) at an initial strain rate of 2.5×10^{-4} s^{-1}. The primary results shown that the structural inhomogeneity strongly controls the ductility of $Cu_{47.5}Zr_{47.5}Al_5$ BMG. Second, mechanical treatments as cold rolling can induce structural inhomogeneity. Some of the data are still in work, because they have to be correlated with the mechanical behavior, as it was done for Fe-based alloy systems.

The typical brittle behavior of metallic glasses can be overcome with in-situ crystallization of ductile phases in the glassy matrix [21]. Between these composites, the shape memory bulk metallic glass composites (BMGC) are unique since they can exhibit a high strength with significant tensile ductility, displaying a work-hardening behavior which is essential for future structural applications [22]. The traditional examples are the CuZr-based BMGC in which a cubic B2-CuZr phase undergoes a martensitic transformation during loading [23]. A new generation of shape memory BMGC based in the B2-CoZr and B2-TiNi phases are being developed but the mechanisms associated with the crystallization of these new alloys still need to be understood. High-energy synchrotron X-ray diffraction was used to study the crystallization mechanisms of four Cu-Zr-Co and Ti-Cu-Ni glassy ribbons. The samples were heated at constant heat of 20 K/min and diffractograms were taken using an acquisition time of 20 seconds. Fig. 8 shows the results for $Ti_{50}Cu_{43}Ni_7$ and $Cu_{42.5}Zr_{45}Co_{12.5}$. The $Ti_{50}Cu_{43}Ni_7$ alloy crystallizes in two steps as indicated in the DSC curve (Fig. 8 a) with a small amount of B2-TiNi phase precipitating first followed by B11-TiCu phase (Fig. 8 b). The inset of Fig. 8 (b) shows in-situ B2-CoZr nanocrystallization in the $Cu_{42.5}Zr_{45}Co_{12.5}$ glassy ribbon at temperature between the glass transition and the crystallization temperature.

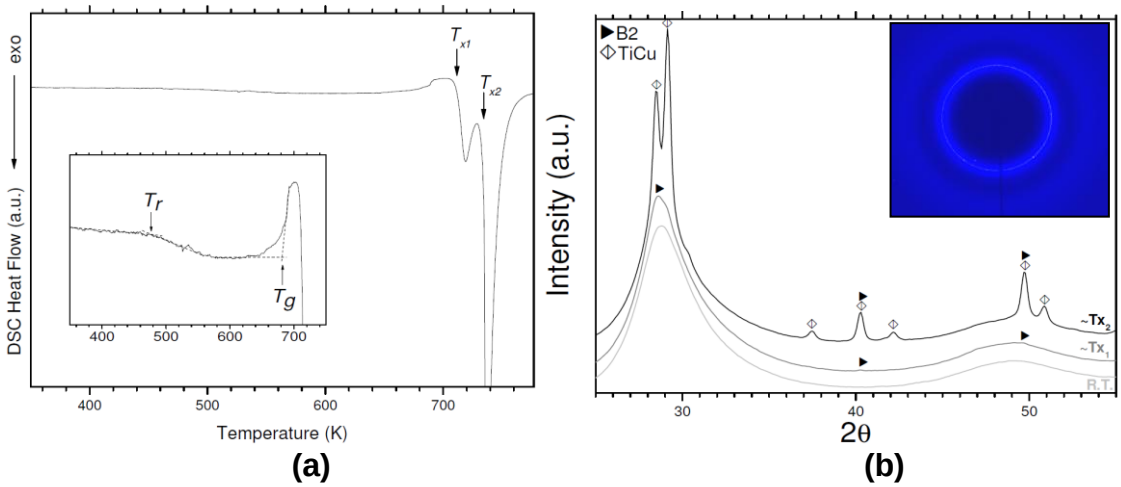

Figure 8 (a) DSC curve of $Ti_{50}Cu_{43}Ni_7$ glassy ribbon at 30 K/min and (b) the diffractograms obtained at room, first and second onset crystallization temperature (T_{x1} and T_{x2}). Inset: Diffractogram of the $Cu_{42.5}Zr_{45}Co_{12.5}$ ribbon taken at 720K exhibiting nanocrystallization of the B2-CoZr phase.

Other investigated system was Al-Cu-Fe, which usually develop a quasicrystalline structure upon milling. The structure evolution of the Al-Cu-Fe quasicrystalline phase during mechanical milling is presented in Fig. 9. The XRD pattern of the starting as-prepared sample (0 h) is characterized by several distinct and sharp diffraction peaks that can all unambiguously be ascribed to the face centered icosahedral (FCI) $Al_{62.5}Cu_{25}Fe_{12.5}$ quasicrystalline phase. No additional diffraction peaks can be observed, implying that the $Al_{62.5}Cu_{25}Fe_{12.5}$ is the only phase present. The patterns of the milled sample display a noticeable broadening of the diffraction signals, which intensifies with increasing of the milling time. This indicates that a strong decrease of the grain size occur during milling.

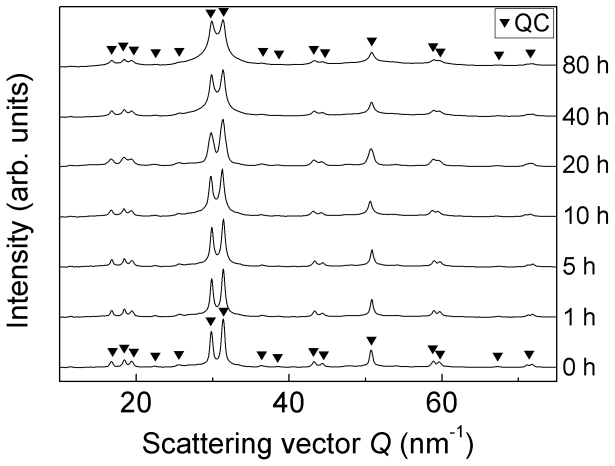

Fig. 9 Structure evolution of the Al-Cu-Fe quasicrystalline phase during mechanical milling is presented.

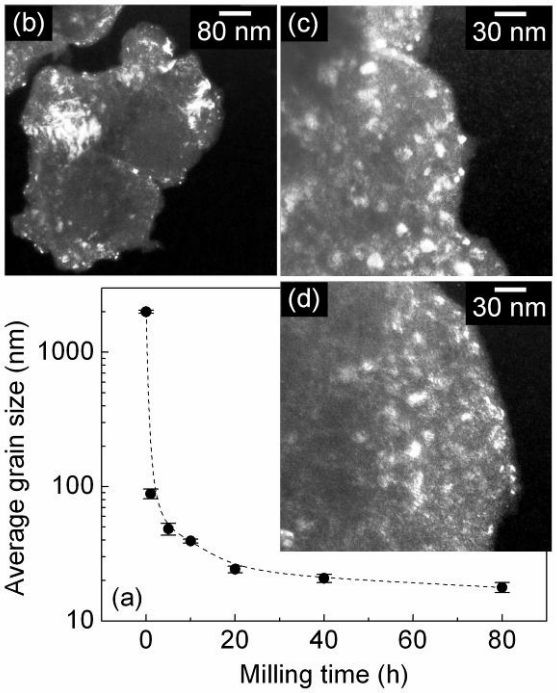

Fig. 10 Grain size and TEM micrographs of milled QC powders.

In order to further evaluate the evolution of the grain size during milling, the samples milled for different periods were investigated by TEM. The average grain size of the QC phase evaluated by TEM is shown in Fig. 10 (a) as a function of the milling time. The grain size rapidly decreases from ~2 μm for the as-deposited material (0 h) to about 88 after 1 h of mechanical treatment (Fig. 10 (b)). The grain size is further reduced to ~24 nm after milling for 20 h (Fig. 10 (c)). For longer milling times (> 20 h), additional grain refinement

occurs at much slower rate, reaching the minimum value of ~ 18 nm for the powder milled for 80 h (Fig. 10 (d)).

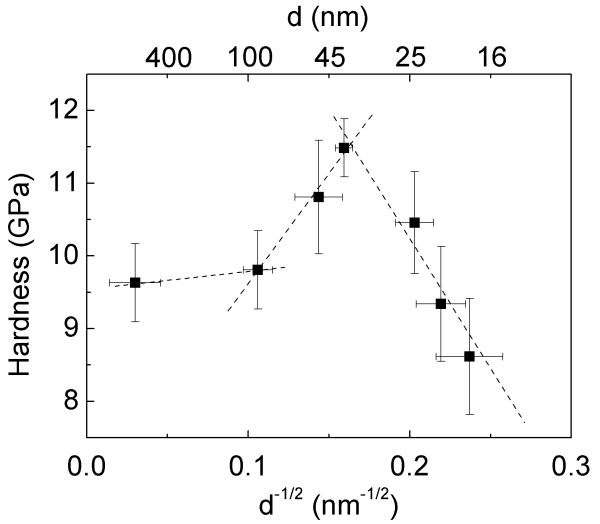

Fig. 11 The hardness of the milled QC powder plotted as a function of $d^{-1/2}$.

Grain size refinement has a significant influence on the hardness of the milled QC powders, as shown in Fig. 11, where the hardness is plotted as a function of $d^{-1/2}$. Two distinct behaviors can be observed: a Hall-Petch behavior for decreasing the grain size from 2000 to 40 nm, where the hardness increases from 9.6 to 11.5 GPa with, and an inverse HP behavior for grain sizes smaller than 40 nm, where the hardness decreases from 11.5 to 8.6 GPa. Interestingly, the HP behavior observed for grain sizes larger than 40 nm is not linear. The hardness initially increases slightly from 9.6 to 9.8 GPa with a slope k = 2.3 GPa/nm$^{1/2}$ for a size reduction from 2000 to 100 nm. This is followed by a second stage between 100 and 40 nm, where the hardness increases more steeply from 9.8 to 11.5 GPa with a slope k = 30 ± 4 GPa/nm$^{1/2}$. The transition between HP to inverse HP behavior occurs at about 40 nm, which represents the critical value for grain size softening of the present $Al_{62.5}Cu_{25}Fe_{12.5}$ quasicrystals. Below 40 nm, the slope of the HP plot becomes negative ($k = -37 \pm 6$ GPa/nm$^{1/2}$).

The x-ray diffraction can be also used to estimate the strain tensor of a sample subjected to an applied load. This method can be applied to reveal the effect of hydrostatic stress state on the atomic scale structural changes in glasses at high pressure, the change in free volume during annealing, the strain in the crystalline phase in glass-matrix composites, as well as for calculating the strain tensor in monolithic BMG below the elastic limit or beyond the Hookean limit [24]. The strain determination of bulk metallic glasses from XRD data is based on concepts previously reported by Poulsen et al. [25]. The symmetric circular diffraction pattern is characterized with respect to the polar coordinates (s ,φ). By dividing the φ range of 0 to 2π into 36 segments, one obtains symmetrized intensity distributions [24, 26]. The relative change in the position of the first peak upon applying an external stress defines the strain ε, which is angular dependent:

$$\varepsilon_i(\varphi_i,\sigma) = \frac{q(\varphi_i,0) - q(\varphi_i,\sigma)}{q(\varphi_i,\sigma)}, \tag{1}$$

The angular variation of the strain can be fitted to the following expression:

$$\varepsilon_\varphi(\varphi,\sigma) = \varepsilon_{11}\sin^2\varphi + \gamma_{12}\sin\varphi\cos\varphi + \varepsilon_{22}\cos^2\varphi \quad . \tag{2}$$

As a result, the strain tensor can be determined, and the axial (ε_{11}), tangential (ε_{22}) and in-plane shear component (γ_{12}) can be derived. Components not in the plane perpendicular to the incoming beam can be determined by rotating the specimen around an axis perpendicular to the incoming beam. However, in the case of amorphous alloys this is not necessary since their structure is highly isotropic. This method was never applied in order to estimate the residual stress and the residual strain induced by plastic deformation. For studying this process, we prepared at the home Institute (IFW Dresden) a slice of a Zr-based BMG which was further mechanical deformed by creating equidistant indentation. The cross-section of the sample was scanned vertically and horizontal, as it is depicted in Fig. 12. The x-ray beam passed through the sample parallel with the indents. The red lines on top symbolize the places where the BMG plate was intended (plastically deformed).

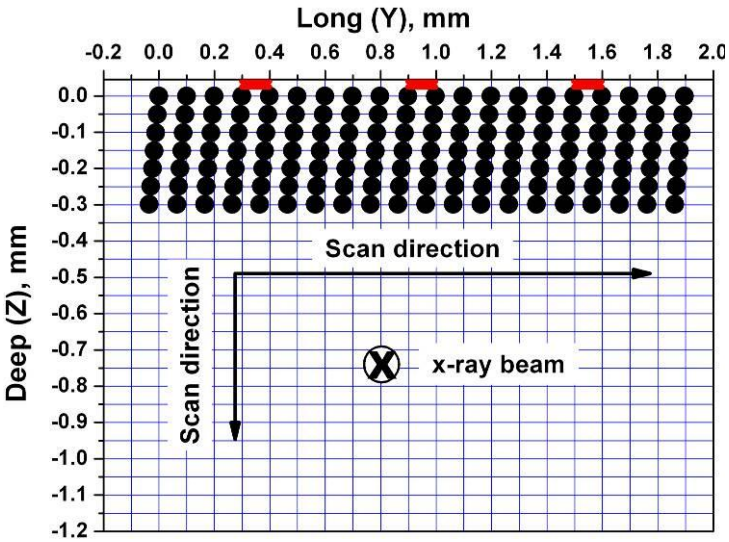

Fig. 12 Scan procedure of a 2mm x 1mm BMG plate plastically deformed (indented).

Following the mechanism described earlier, we plotted the *Q* positions of the first diffraction maximum as a function of the long direction (Y axis in Fig. 12). Line stands for the each scanned line in the deep direction (Z axis in Fig. 12). The data were considered for 6 scanned lines, from 2 to 7 if one considers the Fig. 12. The very first scanned layer was not taken in consideration because there the thickness of the irradiated material was both constant (due to the indentations). Basically for this experiment we scanned not only the indented sample but also the as-cast one. For comparison, Fig. 13 shows the Q positions for both, as-cast (AC) and indented (IND) samples. There one can clearly see a huge variation of the Q for the indented sample when compared with the as-cast sample. This clearly indicates the residual stress and, implicitly, residual strain in the indented sample. With the help of those data we were able to create a map of the stress distribution in the sample, as presented in Fig. 14. there it is very interesting to see how the strain changes the sign (i.e. from compressive to tensile) in the vicinity of the indents. All these data will help to understand the mechanism of the plastic deformation of the metallic glasses and will help to design new methods to enhance the BMGs ductility.

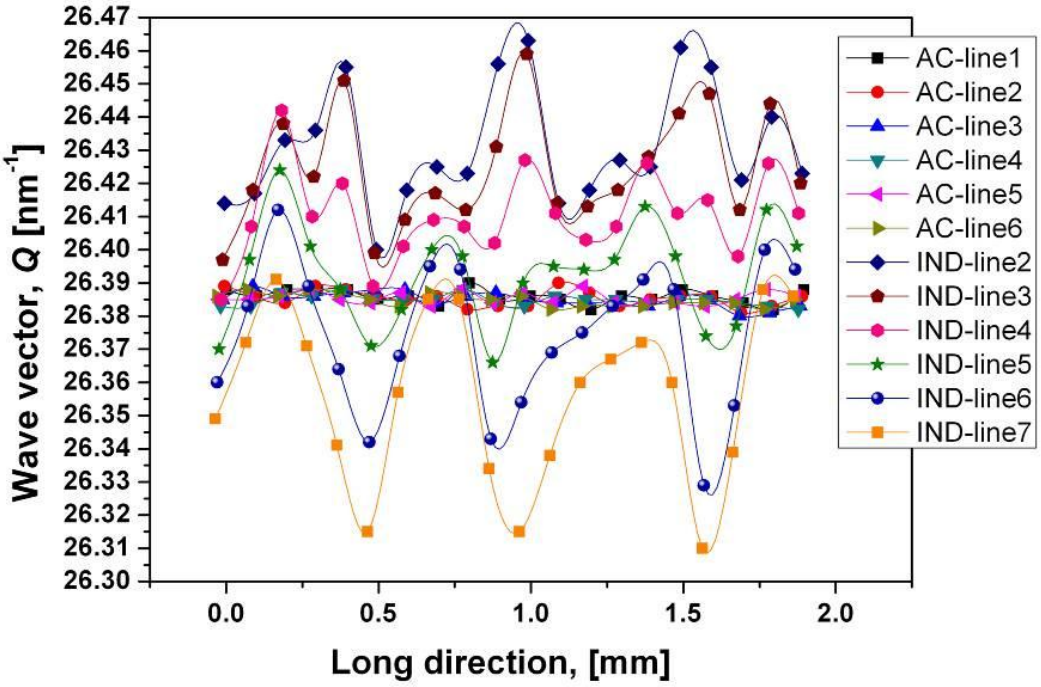

Fig. 13 the Q positions for both, as-cast (AC) and indented (IND) samples.

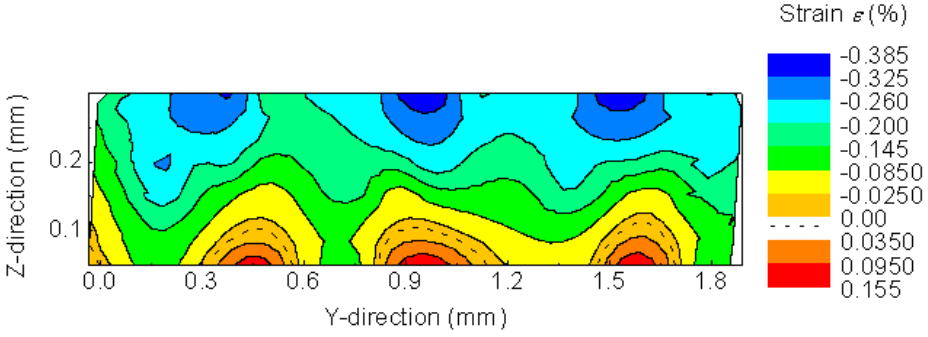

Fig. 14 Map of the residual strain distribution

The collected data during the experiment HD 482 were presented or will be presented at prestigious international Conferences and published in peer-reviewed journals (and not only, here are just few examples for the short-medium term):
- ISMANAM 2011 Gijon, Spain, July 2011 (two oral presentations).
- EUROMAT 2011, Montpellier, France, 12-15 September 2011 (two oral presentations).
- RQ 14, Salvador, Brazil, (two invited talks).
Papers which are sent to Journals or in preparation:
- "The nature of the ductile to brittle transition in Fe83B17 glassy alloy and the role of the emerging Fe23B6 intermetallic phase" K. Georgarakis, YF Guo, M Stoica, G. Vaughan, A.R. Yavari.
- "Thermal behavior of Pd40Cu30Ni10P20 bulk metallic glasses" N. Mattern, M. Stoica, G. Vaughan, J. Eckert, manuscript sent to Acta Materialia.

References

[1]. Wu TW, Spaepen F. Philos Mag B;61 (1990) 739.
[2]. Yavari, A.R., J. of Mat. Res., 1 (1986) 746.
[3]. Yavari, A.R., Mat Sci & Engineer., 98 (1988) 491.
[4]. Aljerf M., Georgarakis K., Yavari AR, Acta Met. 59 (2011) 3817.
[5]. N.Mattern, J. Eckert, U. Kühn, H. Hermann, J. Sakowski, G. Herms, J. Neuefeind, Appl.Phys.Let. 80 (2002) 4225-4227
[6]. A.R. Yavari, A. Le Moulec, A. Inoue, N. Nishiyama, N. Lupu, E. Matsubara, W.J. Botta, G. Vaughan, M. Di Michiel, A. Kvick, Acta Mater. 53 (2005) 1611–1619.
[7]. D.V. Louzguine, A.R. Yavari, K. Ota, G. Vaughan, A. Inoue, J. Non-Cryst. Solids 351 (2005) 1639–1645.
[8]. R.T. Ott , M.J. Kramer, M.F. Besser , D.J. Sordelet, Acta Materialia 54 (2006) 2463–2471
[9]. Louzguine-Luzgin DV, Inoue A, A.R. Yavari , Vaughan G, APPLIED PHYSICS LETTERS Volume: 88 Issue: 12 Article Number: 121926 (2006)
[10]. Dmitri V. Louzguine-Luzgin , Alain Reza Yavari , Mikio Fukuhara , Katsumi Ota ,Guoqiang Xie , Gavin Vaughan , Akihisa Inoue , Journal of Alloys and Compounds 431 (2007) 136–140
[11]. W.J. Botta , K. Ota, K. Hajlaoui , G. Vaughan , A.R. Yavari Journal of Non-Crystalline Solids 354 (2008) 325–327
[12]. Yan Li , Konstantinos Georgarakis, Shujie Pang , Chaoli Maa, Gavin Vaughan , Alain Reza Yavari , Tao Zhang
INTERMETALLICS Volume: 17 Issue: 4 Pages: 231-234 Published: APR 2009
[13]. E. Pineda, I. Hidalgo, P. Brun, T. Pradell a,d, A. Labradore, D. Crespo, Journal of Alloys and Compounds 483 (2009) 578–581
[14]. K. Hajlaoui, M. A. Yousfi, Z. Tourki, G. Vaughan, A. R. Yavari , J Mater Sci (2010) 45:3344–3349
[15]. J. Bednarcik, S. Michalik, M. Sikorski, C. Curfs, XD. Wang, J.Z.Jiang, H. Franz , J. Phys.: Condens. Matter 23 (2011) 254204
[16]. K. Hajlaoui; M. A. Yousfi; I. Ouelhazi; K. Georgarakis; Z. Tourki; G. Vaughan; A. R. Yavari, PHILOSOPHICAL MAGAZINE LETTERS Volume: 91 Issue: 2 Pages: 122-133 Published: 2011
[17]. Y.Waseda, T. Egami, JOURNAL OF MATERIALS SCIENCE 14 (1979) 1249-1253
[18]. H.S. CHEN, K. T. AUST, Y. WASEDA, JOURNAL OF MATERIALS SCIENCE LETTERS 2 (1 9 8 3) 153-157
[19]. S. Kondo, K. Tateishi, N. Ishizawa, Jpn. J. Appl. Phys. 47 (2008) pp. 616-619.
[20]. Peng HL, Li MZ, and Wang WH. Phys Rev Lett 2011;106:135503.
[21]. Eckert J, Das J, Pauly S, Duhamel C. Journal of Materials Research 2007;22:285.
[22]. Hofmann DC. Science 2010;329:1294.
[23]. Pauly S, Das J, Bednarcik J, Mattern N, Kim KB, Kim DH, Eckert J. Scripta Materialia 2009;60:431.
[24]. M. Stoica, J. Das, J. Bednarčik, H. Franz, N. Mattern, W. H. Wang, J. Eckert, J. Appl. Phys. 104, 013522 (2008).
[25]. H.F. Poulsen, J.A. Wert, J. Neuefeind, V. Honkimäki, M. Daymond, Nat. Mater. 4, 33 (2005).
[26] M. Stoica et al., "Mechanical Response of Metallic Glasses: Insights from In-situ High Energy X-ray Diffraction"- Research Summary, JOM vol. 62, p. 76, 2010.